HHS Public Access

Author manuscript

ACS Biomater Sci Eng. Author manuscript; available in PMC 2018 June 06.

Published in final edited form as:

ACS Biomater Sci Eng. 2017 February 13; 3(2): 153–159. doi:10.1021/acsbiomaterials.6b00438.

Flexible Macromolecule versus Rigid Particle Retention in the Injected Skin and Accumulation in Draining Lymph Nodes Are Differentially Influenced by Hydrodynamic Size

Nathan Andrew Rohner[†,‡] and **Susan Napier Thomas**[†,‡,§,||,*]

[†]George W. Woodruff School of Mechanical Engineering, Georgia Institute of Technology, 801 Ferst Drive, Atlanta, Georgia 30332, United States

[‡]Parker H. Petit Institute for Bioengineering and Bioscience, Georgia Institute of Technology, 315 Ferst Drive, Atlanta, Georgia 30332, United States

[§]Wallace H. Coulter Department of Biomedical Engineering, Georgia Institute of Technology and Emory University, Atlanta, Georgia 30332, United States

[||]Winship Cancer Institute, Emory University School of Medicine, 1365-C Clifton Road Northeast, Atlanta, Georgia 30322, United States

Abstract

Therapeutic immunomodulation in the skin, its draining lymph nodes, or both tissues simultaneously using an intradermal administration scheme is desirable for a variety of therapeutic scenarios. To inform how drug carriers comprising engineered biomaterials can be leveraged to improve treatment efficacy by enhancing the selective accumulation or retention of payload within these target tissues, we analyzed the influence of particle versus macromolecule hydrodynamic size on profiles of retention in the site of dermal injection as well as the corresponding extent of accumulation in draining lymph nodes and systemic off-target tissues. Using a panel of fluorescently labeled tracers comprising inert polymers that are resistant to hydrolysis and proteolytic degradation that span a size range of widely used drug carrier systems, we find that macromolecule but not rigid particle retention within the skin is size-dependent, whereas the relative dermal enrichment compared to systemic tissues increases with size for both tracer types. Additionally, macromolecules 10 nm in hydrodynamic size and greater accumulate in draining lymph nodes more extensively and selectively than particles, suggesting that intra- versus extracellular availability of delivered payload within draining lymph nodes may be influenced by both the size and form of engineered drug carriers. Our results inform how biomaterial-based drug

[*]Corresponding Author: susan.thomas@gatech.edu. Tel: +1 (404) 385-1126. Fax: +1 (404) 385-1397.

ORCID

Nathan Andrew Rohner: 0000-0002-9112-2382

Author Contributions

All authors contributed to the experimental design, figure generation, and writing of the manuscript. All authors have revised and approved the final version of the manuscript.

Notes

The authors declare no competing financial interest.

Supporting Information

The Supporting Information is available free of charge on the ACS Publications website at DOI: 10.1021/acsbiomaterials.6b00438.

Individual versus mixture fluorescent tracer characterization and column chromatography experiments (PDF)

carriers can be designed to enhance the selective exposure of formulated drug in target tissues to improve the therapeutic efficacy as well as minimize off-target effects of locoregional immunotherapy.

Graphical Abstract

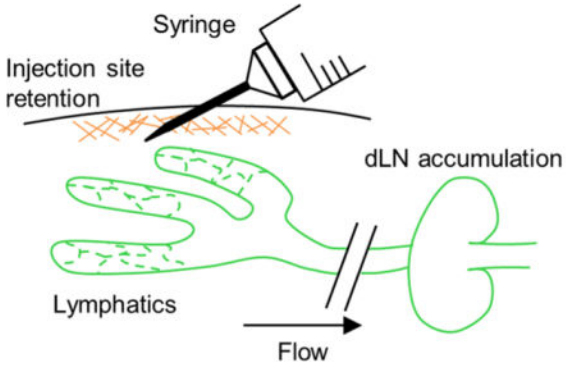

Keywords

biodistribution; intradermal; drug delivery; lymphatic

INTRODUCTION

Immunotherapy is increasingly employed for the treatment of a variety of pathologies, such as cancer and autoimmune disease. Accordingly, biomaterial-based formulation approaches have been explored to improve the bioactivity and therapeutic efficacy of numerous immunotherapeutic interventions.[1–3] These include strategies to codeliver multiple immunotherapeutic drugs,[4,5] provide sustained and/or controlled drug release,[6–8] and improve drug circulation half-lives,[4,9,10] the success of which are critically influenced by the adequate and selective accumulation or retention of drug within target tissues. To this end, biomaterials have been used to improve drug bioavailability within healthy[11,12] and diseased skin,[13–15] key targets in vaccine, skin graft, and cancer immunotherapy applications. Notwithstanding approaches leveraging the enhanced permeability and retention effect for tumor-enhanced delivery after intravenous injection, dermal delivery is largely accomplished via direct injection.[13,14] Consequently, designing drug carriers to achieve prolonged retention at the site of injection has been widely explored to improve drug bioavailability and potency.[11,14]

Lymph nodes (LNs) are emerging as key immunotherapeutic targets given their role in directing adaptive immunity and tolerance.[16–18] Notably, the efficacy of infectious disease and cancer vaccines is improved by LN-targeting[19–23] resulting from the localized modulation of immunological signaling to alter adaptive immune response. As an example of such an approach, delivery to melanoma draining LN (dLN) mediated by lymphatic-draining synthetic polymer nanoparticles improves adjuvant activity, in particular increasing dendritic cell maturation as well as Th1 and antitumor $CD8^+$ T cell immunity, resulting in

reduced tumor growth, a response lost by adjuvant delivery in a nontargeted manner or to LN not draining the melanoma.[19] In another example, corticosteroid delivery to skin graft dLN mediated by encapsulation within block copolymer micelles has demonstrated success in delaying rejection.[24] Localizing drug activity to dLN can thus provide significant advantages to immunotherapy in improving immunological outcomes in addition to achieving dose sparing to minimize off target effects/toxicities.[25,26]

Given the local immunological signaling associated with pathogenesis in both the diseased skin and its dLN, therapeutic immunomodulation in either the skin or its dLN or, conversely, in both tissues simultaneously is potentially desirable for numerous therapeutic scenarios. However, despite recent advances in targeted immunotherapeutics using biomaterials,[22,23,25,27] there is limited understanding of how carrier design simultaneously affects retention and accumulation in both the skin injection site and its dLN. Previous studies have explored the effects of biomaterial carrier size,[21,28] charge,[29,30] hydrophobicity,[31,32] and shape[33,34] on various aspects of transport, cellular uptake, and adaptive immune response. How the coupled effects of both size and form influence carrier transport, especially with respect to dermal and dLN targeted applications, however, remains to be described. Since biomaterial-based delivery systems are increasingly explored for immunotherapeutic delivery,[3,35] we sought to analyze the differences in profiles of spherical particulate versus macromolecular retention as a function of hydrodynamic size in the site of dermal injection as well as the corresponding extent of accumulation in dLN and systemic off-target tissues. This was achieved by implementing a panel of tracers comprised of inert polymers (polystyrene particles and dextran macromolecules) that are resistant to hydrolysis and proteolytic degradation that span a size range of widely used drug carrier systems and are labeled with fluorophores with minimal tissue absorbance and spectral overlap.[36] Tracers were intradermally infused into naïve C57Bl6 mice and their biodistribution among the skin injection site, dLN, and systemic tissues was examined by end point analysis and fluorescent measurement of homogenized tissues. Our results demonstrate that chain-like, flexible macromolecular but not rigid, spherical particulate retention within the skin injection site is size-dependent, that enrichment within the skin relative to systemic tissues increases with size for both macromolecules and particles, and macromolecules accumulate in dLN more extensively and selectively than rigid, spherical particles.

MATERIALS AND METHODS

Fluorescent Tracers

Fluorescein isothiocyanate labeled 2 MDa dextran was purchased from Sigma-Aldrich (St. Louis, MO, USA); 500, 50, and 25 nm fluorescent (580/610 nm, 660/680 nm, and 625/ 645 nm excitation/emission, respectively) carboxylate-modified polystyrene microspheres and 70 and 40 kDa fluorescent (490/520 nm and 555/585 nm excitation/emission, respectively) dextrans were purchased from Thermo Fisher Scientific (Waltham, MA, USA). 500 kDa or 10 kDa amine-dextrans (Sigma-Aldrich) were covalently labeled by incubation in 0.1 M $NaHCO_3$ buffer at pH 8.4 for 4 h with Alexa Fluor 700 *N*-hydroxysuccinimide (NHS) ester or Alexa Fluor 610-X NHS-ester dye (Thermo Fisher Scientific), respectively. Individual fluorescent dextran conjugates were purified from unreacted free dye and confirmed to be

free of unconjugated dye by Sepharose CL-6B gravity column chromatography as previously described.[36] All reagents were maintained and used under sterile conditions. Hydrodynamic sizes of individual fluorescently conjugated tracers were measured by dynamic light scattering using a Zetasizer Nano ZS (Malvern Instruments Ltd., Malvern, United Kingdom), except for the 25 nm polystyrene spheres for which the manufacturer's sizing data were used because of fluorophore incompatibility with our Zetasizer Nano ZS.

Biodistribution Experiments and Analysis

C57Bl6 mice were purchased from Jackson Laboratories (Bar Harbor, ME, USA). All protocols were approved by the Institutional Animal Care and Use Committee. Thirty μL of fluorescent tracer solution normalized for equivalent material volumes using the respective radius or hydrodynamic radius (either 1.2×10^8 500 nm spheres, 7.9×10^{11} 50 nm spheres, 23.8 μg of 500 kDa AF700-dextran, and 3 μg of 10 kDa AF610-dextran ($n = 9$ for 24 h, $n = 9$ for 72 h in 6 independent experiments); or 8.3×10^{11} 25 nm spheres and 1.38 μg of 2 MDa FITC-dextran ($n = 3$ for 24 h, $n = 6$ for 72 h in 4 independent experiments); or 8.3×10^{11} 25 nm spheres, 1.93 μg of 40 kDa TRITC-dextran and 0.81 μg of 70 kDa FITC-dextran ($n = 3$ for 24 h, $n = 3$ for 72 h in 4 independent experiments)) in saline was infused intradermally into the shaved lateral dorsal skin using a syringe pump at a rate of ~300 nL per sec as previously described.[36] Tracers with similar labels were injected into separate animal cohorts. Twenty-four or 72 h post injection (p.i.), the brachial LNs ipsilateral and contralateral to the site of injection, the skin at the injection site, and the spleen, lungs, liver, and kidneys were harvested and homogenized in D-PBS using 1.4 mm acid washed zirconium grinding beads (OPS Diagnostics LLC, Lebanon, NJ, USA) with a FastPrep-24 Automated Homogenizer (MP Biomedicals, Santa Ana, CA, USA). Tissue homogenate fluorescence was measured using a Synergy H4 BioTek plate reader (BioTek Instruments Inc.), compensation for fluorescence overlap was applied, and fluorescent tracer standard curves were made in individual tissue homogenates. Concentrations were calculated as the percent of tracer injection amount per whole tissue volume (%/mL). Prism 6 (GraphPad Software Inc., La Jolla, CA, USA) was used to calculate exposure from the area under the curve (AUC) of tracer concentrations measured between 0 and 72 h. Error propagation analysis was used to calculate AUC standard error. Systemic tissues used in ratio calculations included the spleen, lungs, liver, and kidneys. Due to high systemic tissue (spleen, lungs, liver, and kidneys) autofluorescence around FITC wavelengths, FITC labeled tracers (70 kDa and 2 MDa dextrans) were not included in concentration ratio analyses.

Statistical Analysis

Data are represented as the mean with standard error. Statistics were calculated and linear regressions were performed using Prism 6 (GraphPad Software Inc.). Statistical significance was defined as $p < 0.05$ following Mann–Whitney U tests or one-way ANOVA followed by Fisher's Least Significant Difference (LSD) test. One, two, and three symbols denoting statistical significance represent $p < 0.05$, 0.01, and 0.001, respectively, unless otherwise specified.

RESULTS

Skin Retention versus Exposure in Systemic Tissues Increases with Increasing Tracer Size

A panel of eight dextran and polystyrene sphere tracers spanning 5–54 and 25–500 nm in hydrodynamic diameter, respectively (Figure 1A, B), was used to interrogate the effect of size versus form on skin retention and biodistribution. Because we wanted to explore whether size-based principles of dLN drug delivery are similar for macromolecule- and particle-based delivery systems, two size-matched tracer subsets in the size range of passive lymphatic transport (25 nm polystyrene vs 30 nm dextran and 50 nm polystyrene vs 54 nm dextran) were used to enable the direct comparison of carrier form on dermal retention and dLN accumulation. Five nm dextran and 500 nm polystyrene spheres were also included as benchmarks for modes of tracer transport from the interstitium besides passive lymphatic uptake for tracers with low retention at the site of injection due to absorption into the bloodstream and requiring active cell-mediated transport from the site of injection to the dLN, respectively. Measured profiles of biodistribution (Figure S1A) and size-exclusion column chromatography elution (Figure S1B) confirmed that individually versus coinfused tracers behaved identically with minimal to no interaction or aggregation effects.

After infusion into the skin, the smallest (5 nm) dextran was cleared most quickly from the injection site, with less than 5% of the injected amount remaining after 24 h and only approximately 3% left at 72 h p.i. (Figure 2A). In contrast, around 20–40% of the 10 and 12 nm dextrans, 50% of the 30 nm dextran, and 85–100% of the 25–500 nm polystyrene sphere and 54 nm dextran tracers were measured in the dermis at 24 and 72 h p.i. (Figure 2A). As a result, the concentrations of the larger tracers (25, 50, 54, and 500 nm) in the skin were significantly greater than that of the 5, 10, and 12 nm dextran at 24 and 72 h p.i. (Figure 2A). When also considering the concentration of tracer that accumulated in systemic tissues, the relative amount of tracer localized to the skin tissue surrounding the site of skin injection versus systemic organs increased with tracer size for dextrans 24 h p.i. ($p = 0.050$) and increased for both dextrans ($p = 0.006$) and polystyrene spheres ($p = 0.001$) 72 h p.i. (Figure 2B). The fold enrichment also increased over time, presumably because of tracer elimination via excretion,[37] save for the 25 nm polystyrene spheres (Figure 2B).

Accumulation within dLN is Greatest for Macromolecules and Increases Most Appreciably with Size over 72 h for Particles, Albeit at Lower Levels of dLN-Specific Enrichment Relative to Macromolecules

We next evaluated the extent of tracer accumulation within LN draining the injected skin. We found 30 nm dextran to exhibit the highest levels of dLN accumulation (~2% of injected tracer, approximately 10–20 fold higher than 5 nm dextran or polystyrene sphere tracers of other sizes) at 24 and 72 h p.i. (Figure 3A). Dextrans 10, 12, and 54 nm in hydrodynamic diameter also accumulated within dLN at appreciable levels (~1%), approximately half the amount of 30 nm dextran and when similarly sized, accumulated within LN at 5–10-fold higher levels relative to polystyrene spheres (Figure 3A). Five nm dextran, on the other hand, and 25, 50, and 500 nm polystyrene spheres accumulated in dLN the least at both 24 and 72 h p.i. (Figure 3A). However, the difference in dLN accumulation between 24 and 72 h p.i. significantly increased with polystyrene sphere size ($p = 0.037$) presumably because of

the increasing dependency on cell-mediated trafficking to dLN,[28] with 500 nm polystyrene spheres exhibiting an almost 40 fold change (Figure 3B). The dextran tracers' dLN accumulation, however, remained relatively constant from 24 to 72 h p.i. (Figure 3B), suggesting a sustained, primarily passive lymphatic transport mechanism.[38] When compared to concentrations of tracers accumulating in systemic tissues, the 30 nm dextran demonstrated the highest dLN/systemic ratio at 24 and 72 h p.i., around one to 2 orders of magnitude over that of the other dextran tracers, and interestingly, an order of magnitude higher than the similarly sized 25 nm polystyrene sphere tracer (Figure 3C). Considering concentrations of tracers accumulating in dLN relative to those in both skin and systemic tissues, dextran tracers exhibited an order of magnitude higher dLN enrichment, whereas the polystyrene tracers exhibited ratios at or less than one (Figure 3D). We also found higher levels of 30 nm dextran tracer accumulation within dLN relative to the skin and systemic tissues as compared to size-matched polystyrene spheres at 24 h p.i. (Figure 3D).

Macromolecular but Not Particulate Tracer Exposure within the Skin and dLN is Size-Dependent

Lastly, we sought to evaluate the effects of tracer size and form on total exposure (e.g., AUC) within the site of skin injection and the dLN from 0 to 72 h p.i.. We found that skin exposure to injected dextran but not polystyrene sphere tracers increased with hydrodynamic size ($p = 0.022$), reaching levels similar to that measured for all polystyrene tracers (Figure 4A). The dextrans 10–54 nm in hydrodynamic diameter also exhibited the highest levels of exposure within LN draining the injected skin, levels up to 4-fold higher than those measured in the skin itself and greatest for the 30 nm dextran tracer (Figure 4B). Contrastingly, polystyrene sphere tracer exposure within the injected skin was similar to the largest (54 nm) dextran tested and dLN exposure was similar irrespective of size and at levels similar to those found for the dextran tracer exhibiting the lowest exposure in dLN (5 nm, Figures 4A, B). Accordingly, the exposure of size-matched dextran and polystyrene tracers was similar in the skin but significantly greater (~3 to 10-fold) in dLN for both sizes of dextrans relative to the polystyrene spheres (Figure 4B, C). Taken together, when simultaneously considering exposure within the dLN versus skin, three separate tracer groups of dLN versus skin exposure emerged: the small macromolecule 5 nm dextran exhibited low exposure in both the dLN and skin, intermediate sized macromolecules (10–54 nm dextrans) exhibited high exposure in both dLN exposure and skin (10–20-fold and 5–10-fold relative to 5 nm dextran, respectively), and particles of all tested sizes (25–500 nm polystyrene tracers) displayed low dLN exposure at levels similar to those seen with 5 nm dextran but 7–10-fold higher levels of skin exposure (Figure 4D).

DISCUSSION

Biomaterials-based formulation strategies offer numerous advantages for the maximization of immunotherapeutic drug bioavailability in target tissues[7,9,14,28] while simultaneously limiting off-target effects.[14,25,26] Design criteria for increasing the efficiency and selectivity of agent delivery or retention in order to prolong drug exposure in skin and dLN, tissue targets in a variety of immunotherapeutic regimens (e.g., intra-lymphatic immunotherapy[39,40] as well as intradermal (or intralesional) injection for allergic contact

dermatitis and plaque psoriasis[41] or oncolytic virus therapy in melanoma,[42] respectfully), using biomaterials thus has the potential to increase treatment efficacy, reduce off-target effects, and potentially eliminate the need for repeated local injections.[43–45]

In this study, we explored the effects of macromolecular versus particulate size on profiles of skin retention and selectivity of dLN accumulation. A range of fluorescent tracer sizes relevant to engineered macromolecular and particulate drug carriers was implemented and the time points of analysis (24 and 72 h p.i.) were chosen to allow the interrogation of both lymphatic transport mechanisms: cell-mediated uptake and migration which peaks 2–4 days p.i.[46,47] versus passive lymphatic drainage from the interstitial injection site.[16,19,48–50] Corroborating earlier reports,[36,51] we find retention within the injected skin to be size-dependent (Figure 2A), as is the relative selectivity of skin exposure to injected agent relative to systemic tissues (Figure 2B). When size matched, macromolecular and particulate retention in the skin is equivalent (Figure 2A), resulting in similar, although somewhat higher in the case of ~25–30 nm sized tracers, skin exposure (Figure 4C). Levels of dLN accumulation were higher for dextrans relative to polystyrene spheres at all tested sizes, save 5 nm dextran (Figure 3A). However, the specificity of dLN accumulation relative to systemic tissues was highest for an intermediate-sized (30 nm) dextran and at 72 h p.i. for the largest (500 nm) polystyrene sphere tested (Figure 3C), presumably because of these tracers exhibiting the most robust levels of lymphatic uptake[52] versus high level of retention within (Figure 2A) and restriction to (Figure 2B) the skin as well as dependency of the 500 nm tracer on cell-mediated transport to dLN (Figure 3B). Furthermore, macromolecular tracers accumulated in dLN at levels roughly ten times that of size-matched polystyrene spheres (Figure 4B–D). Therefore, the interplay among hydrodynamic size and flexible, chainlike macromolecular versus rigid, spherical particulate form control the exposure at the site of skin injection versus simultaneous capacity to deliver payload to dLN, respectively. As previous studies[19,23] have demonstrated that the extent of LN delivery influences immunotherapeutic outcomes,[19,23] we show herein the importance of considering the coupled effects of both the size and form/flexibility of biomaterial carriers to potentially increase therapeutic efficacy in vaccine or immunotherapy applications.

Since after cellular uptake, drug carriers and their payload are presumably restricted to within migrating cells,[53] the mechanism of lymphatic-mediated delivery to dLN influences the signaling capacity of and the availability of intra- versus extracellular drug targets in migrating versus LN-resident cells to delivered payload.[28] Our results suggest that since dextran tracer concentrations in the dLN did not increase from 24 to 72 h p.i. (Figures 3A, B), macromolecular transport from the skin to the dLN is primarily mediated via passive lymphatic drainage and is thus largely extracellularly available. Despite much lower total levels of dLN accumulation relative to tested dextrans, the same likely also holds for 25 nm polystyrene spheres (Figure 3B). However, the 50 and 500 nm polystyrene tracers exhibited an increase of approximately 5- and 40-fold, respectively, by 72 h p.i. (Figure 3B), and are thus, in part, restricted within dLN to the cells that migrated there from the periphery. These results corroborate previous work demonstrating that accumulation of large (500 and 1000 nm) particles within dLN is cell-mediated and absent in dendritic cell-depleted mice[28] or in mice lacking dermal lymphatics,[48,54] whereas smaller (20 nm) particles are still able to drain in dendritic cell-depleted mice and be taken up by a variety of dLN-resident cells.[28]

Together, these results demonstrate that both the size and form of biomaterial drug carriers may impact levels and intra- versus extracellular locality of payload within dLN.

Our results demonstrate the unexplored importance of carrier form for dermal and LN targeting applications as we noted a divergence between the size-dependency of macromolecule and rigid particle profiles of bioavailability within the skin and dLN. Most noteworthy, more than 2% of the injected 30 nm dextran accumulated within the dLN, while dLN accumulation was only 0.2% of the injected amount for similarly sized 25 nm polystyrene spheres. We hypothesize these differences manifest as a result of the increased flexibility of chain-like macromolecular dextrans relative to that of rigid polystyrene spheres,[55–57] as differences in flexibility have been shown to influence both diffusion within skin[58] and lymphatic uptake.[52] How biomaterial rigidity and deformability influence the distribution of drug carriers throughout dLN as well as resulting profiles of resident cell uptake has yet to be fully elaborated. Also, whether particles with lower rigidities, such as those comprised of engineered biomaterials[59] rather than polystyrene, or particles with nonspherical shapes, such as rods or discs,[60,61] exhibit size-dependent biodistribution profiles more similar to macromolecules or polystyrene spheres remains to be determined. Lastly, whereas the primary focus of this work was to elucidate the influence of hydrodynamic size and form on skin retention and dLN accumulation, the coupled effects of numerous other characteristics of engineered biomaterial-based drug carriers (charge, shape, lipophilicity, matrix affinity, etc.) likely play a significant role as well and have yet to be systematically analyzed for dermal retention and dLN accumulation.

CONCLUSION

In summary, our results demonstrate that macromolecule and particle retention within the skin as well as accumulation and enrichment in dLN relative to systemic tissues is acutely influenced by hydrodynamic size but in different respects. The maximization of immunotherapeutic drug therapeutic efficacy within the skin and/or dLN as well as simultaneous limiting off-target effects may thus be tailored by changing the size and/or form of engineered biomaterial-based carriers. These results will inform the rational design of drug targeting and delivery strategies to achieve locoregional immunomodulation.

Supplementary Material

Refer to Web version on PubMed Central for supplementary material.

Acknowledgments

This work was supported by National Institutes of Health (NIH) Grant R01CA207619, the NIH Cell and Tissue Engineering Training Grant T32 GM008433, PHS Grant UL1TR000454 from the Clinical and Translational Science Award Program, NIH, National Center for Advancing Translational Sciences, National Science Foundation Award 1342194, and Department of Defense Grant CA150523.

References

1. Hubbell JA, Thomas SN, Swartz MA. Materials engineering for immunomodulation. Nature. 2009; 462(7272):449–460. [PubMed: 19940915]

2. Weber JS, Mule JJ. Cancer immunotherapy meets biomaterials. Nat Biotechnol. 2015; 33(1):44–45. [PubMed: 25574635]
3. Hotaling NA, Tang L, Irvine DJ, Babensee JE. Biomaterial Strategies for Immunomodulation. Annu Rev Biomed Eng. 2015; 17(1):317–349. [PubMed: 26421896]
4. Park J, Wrzesinski SH, Stern E, Look M, Criscione J, Ragheb R, Jay SM, Demento SL, Agawu A, Licona Limon P, Ferrandino AF, Gonzalez D, Habermann A, Flavell RA, Fahmy TM. Combination delivery of TGF-β inhibitor and IL-2 by nanoscale liposomal polymeric gels enhances tumour immunotherapy. Nat Mater. 2012; 11(10):895–905. [PubMed: 22797827]
5. Xu Z, Ramishetti S, Tseng YC, Guo S, Wang Y, Huang L. Multifunctional nanoparticles co-delivering Trp2 peptide and CpG adjuvant induce potent cytotoxic T-lymphocyte response against melanoma and its lung metastasis. J Controlled Release. 2013; 172(1):259–265.
6. Egilmez NK, Jong YS, Iwanuma Y, Jacob JS, Santos CA, Chen FA, Mathiowitz E, Bankert RB. Cytokine immunotherapy of cancer with controlled release biodegradable microspheres in a human tumor xenograft/SCID mouse model. Cancer Immunol Immunother. 1998; 46(1):21–4. [PubMed: 9520288]
7. Sabel MS, Skitzki J, Stoolman L, Egilmez NK, Mathiowitz E, Bailey N, Chang WJ, Chang AE. Intratumoral IL-12 and TNF-alpha-loaded microspheres lead to regression of breast cancer and systemic antitumor immunity. Annals of surgical oncology. 2004; 11(2):147–56. [PubMed: 14761917]
8. Shimizu T, Kishida T, Hasegawa U, Ueda Y, Imanishi J, Yamagishi H, Akiyoshi K, Otsuji E, Mazda O. Nanogel DDS enables sustained release of IL-12 for tumor immunotherapy. Biochem Biophys Res Commun. 2008; 367(2):330–335. [PubMed: 18158918]
9. Melder RJ, Osborn BL, Riccobene T, Kanakaraj P, Wei P, Chen G, Stolow D, Halpern WG, Migone TS, Wang Q, Grzegorzewski KJ, Gallant G. Pharmacokinetics and in vitro and in vivo anti-tumor response of an interleukin-2-human serum albumin fusion protein in mice. Cancer Immunol Immunother. 2005; 54(6):535–47. [PubMed: 15592670]
10. Gillies SD, Lan Y, Hettmann T, Brunkhorst B, Sun Y, Mueller SO, Lo KM. A low-toxicity IL-2-based immunocytokine retains antitumor activity despite its high degree of IL-2 receptor selectivity. Clin Cancer Res. 2011; 17(11):3673–3685. [PubMed: 21531812]
11. Zaric M, Lyubomska O, Touzelet O, Poux C, Al-Zahrani S, Fay F, Wallace L, Terhorst D, Malissen B, Henri S, Power UF, Scott CJ, Donnelly RF, Kissenpfennig A. Skin Dendritic Cell Targeting via Microneedle Arrays Laden with Antigen-Encapsulated Poly-d,l-lactide-co-Glycolide Nanoparticles Induces Efficient Antitumor and Antiviral Immune Responses. ACS Nano. 2013; 7(3):2042–2055. [PubMed: 23373658]
12. Hatzifoti C, Bacon A, Marriott H, Laing P, Heath AW. Liposomal Co-Entrapment of CD40mAb Induces Enhanced IgG Responses against Bacterial Polysaccharide and Protein. PLoS One. 2008; 3(6):e2368. [PubMed: 18523585]
13. Wang C, Ye Y, Hochu GM, Sadeghifar H, Gu Z. Enhanced Cancer Immunotherapy by Microneedle Patch-Assisted Delivery of Anti-PD1 Antibody. Nano Lett. 2016; 16(4):2334–2340. [PubMed: 26999507]
14. Zaharoff DA, Hance KW, Rogers CJ, Schlom J, Greiner JW. Intratumoral immunotherapy of established solid tumors with chitosan/IL-12. J Immunother. 2010; 33(7):697–705. [PubMed: 20664357]
15. Ruiz P, Maldonado P, Hidalgo Y, Gleisner A, Sauma D, Silva C, Saez JJ, Nunez S, Rosemblatt M, Bono MR. Transplant Tolerance: New Insights and Strategies for Long-Term Allograft Acceptance. Clin Dev Immunol. 2013; 2013:15.
16. Thomas SN, Rohner NA, Edwards EE. Implications of Lymphatic Transport to Lymph Nodes in Immunity and Immunotherapy. Annu Rev Biomed Eng. 2016; 18:207. [PubMed: 26928210]
17. Fransen MF, Arens R, Melief CJM. Local targets for immune therapy to cancer: Tumor draining lymph nodes and tumor microenvironment. Int J Cancer. 2013; 132(9):1971–1976. [PubMed: 22858832]
18. Chandrasekaran S, King MR. Microenvironment of Tumor-Draining Lymph Nodes: Opportunities for Liposome-Based Targeted Therapy. Int J Mol Sci. 2014; 15(11):20209–20239. [PubMed: 25380524]

19. Thomas SN, Vokali E, Lund AW, Hubbell JA, Swartz MA. Targeting the tumor-draining lymph node with adjuvanted nanoparticles reshapes the anti-tumor immune response. Biomaterials. 2014; 35(2):814–24. [PubMed: 24144906]
20. Jeanbart L, Ballester M, de Titta A, Corthesy P, Romero P, Hubbell JA, Swartz MA. Enhancing efficacy of anticancer vaccines by targeted delivery to tumor-draining lymph nodes. Cancer Immunol Res. 2014; 2(5):436–47. [PubMed: 24795356]
21. Fifis T, Gamvrellis A, Crimeen-Irwin B, Pietersz GA, Li J, Mottram PL, McKenzie IF, Plebanski M. Size-dependent immunogenicity: therapeutic and protective properties of nano-vaccines against tumors. J Immunol. 2004; 173(5):3148–54. [PubMed: 15322175]
22. Muraoka D, Harada N, Hayashi T, Tahara Y, Momose F, Sawada S, Mukai SA, Akiyoshi K, Shiku H. Nanogel-based immunologically stealth vaccine targets macrophages in the medulla of lymph node and induces potent antitumor immunity. ACS Nano. 2014; 8(9):9209–18. [PubMed: 25180962]
23. Liu H, Moynihan KD, Zheng Y, Szeto GL, Li AV, Huang B, Van Egeren DS, Park C, Irvine DJ. Structure-based Programming of Lymph Node Targeting in Molecular Vaccines. Nature. 2014; 507(7493):519–522. [PubMed: 24531764]
24. Dane KY, Nembrini C, Tomei AA, Eby JK, O'Neil CP, Velluto D, Swartz MA, Inverardi L, Hubbell JA. Nano-sized drug-loaded micelles deliver payload to lymph node immune cells and prolong allograft survival. J Controlled Release. 2011; 156(2):154–160.
25. Bourquin C, Anz D, Zwiorek K, Lanz AL, Fuchs S, Weigel S, Wurzenberger C, von der Borch P, Golic M, Moder S, Winter G, Coester C, Endres S. Targeting CpG Oligonucleotides to the Lymph Node by Nanoparticles Elicits Efficient Antitumoral Immunity. J Immunol. 2008; 181(5):2990–2998. [PubMed: 18713969]
26. Kwong B, Liu H, Irvine DJ. Induction of potent anti-tumor responses while eliminating systemic side effects via liposome-anchored combinatorial immunotherapy. Biomaterials. 2011; 32(22): 5134–5147. [PubMed: 21514665]
27. Peiris PM, Abramowski A, McGinnity J, Doolittle E, Toy R, Gopalakrishnan R, Shah S, Bauer L, Ghaghada KB, Hoimes C, Brady-Kalnay SM, Basilion JP, Griswold MA, Karathanasis E. Treatment of Invasive Brain Tumors Using a Chain-like Nanoparticle. Cancer Res. 2015; 75(7): 1356–1365. [PubMed: 25627979]
28. Manolova V, Flace A, Bauer M, Schwarz K, Saudan P, Bachmann MF. Nanoparticles target distinct dendritic cell populations according to their size. Eur J Immunol. 2008; 38(5):1404–13. [PubMed: 18389478]
29. Foged C, Brodin B, Frokjaer S, Sundblad A. Particle size and surface charge affect particle uptake by human dendritic cells in an in vitro model. Int J Pharm. 2005; 298(2):315–22. [PubMed: 15961266]
30. Fromen CA, Robbins GR, Shen TW, Kai MP, Ting JPY, DeSimone JM. Controlled analysis of nanoparticle charge on mucosal and systemic antibody responses following pulmonary immunization. Proc Natl Acad Sci U S A. 2015; 112(2):488–493. [PubMed: 25548169]
31. Rao DA, Forrest ML, Alani AW, Kwon GS, Robinson JR. Biodegradable PLGA based nanoparticles for sustained regional lymphatic drug delivery. J Pharm Sci. 2010; 99(4):2018–31. [PubMed: 19902520]
32. Moyano DF, Goldsmith M, Solfiell DJ, Landesman-Milo D, Miranda OR, Peer D, Rotello VM. Nanoparticle hydrophobicity dictates immune response. J Am Chem Soc. 2012; 134(9):3965–7. [PubMed: 22339432]
33. Champion JA, Katare YK, Mitragotri S. Particle shape: a new design parameter for micro- and nanoscale drug delivery carriers. J Controlled Release. 2007; 121(1–2):3–9.
34. Sun B, Ji Z, Liao YP, Wang M, Wang X, Dong J, Chang CH, Li R, Zhang H, Nel AE, Xia T. Engineering an effective immune adjuvant by designed control of shape and crystallinity of aluminum oxyhydroxide nanoparticles. ACS Nano. 2013; 7(12):10834–49. [PubMed: 24261790]
35. Fan Y, Moon JJ. Nanoparticle Drug Delivery Systems Designed to Improve Cancer Vaccines and Immunotherapy. Vaccines. 2015; 3(3):662–85. [PubMed: 26350600]

36. Rohner NA, Thomas SN. Melanoma growth effects on molecular clearance from tumors and biodistribution into systemic tissues versus draining lymph nodes. J Controlled Release. 2016; 223:99–108.
37. Mehvar R, Robinson MA, Reynolds JM. Dose dependency of the kinetics of dextrans in rats: effects of molecular weight. J Pharm Sci. 1995; 84(7):815–8. [PubMed: 7562429]
38. Zhuang Y, Ma Y, Wang C, Hai L, Yan C, Zhang Y, Liu F, Cai L. PEGylated cationic liposomes robustly augment vaccine-induced immune responses: Role of lymphatic trafficking and biodistribution. J Controlled Release. 2012; 159(1):135–42.
39. Johansen P, Häffner AC, Koch F, Zepter K, Erdmann I, Maloy K, Simard JJ, Storni T, Senti G, Bot A, Wüthrich B, Kündig TM. Direct intralymphatic injection of peptide vaccines enhances immunogenicity. Eur J Immunol. 2005; 35(2):568–574. [PubMed: 15682446]
40. Senti G, Prinz Vavricka BM, Erdmann I, Diaz MI, Markus R, McCormack SJ, Simard JJ, Wuthrich B, Crameri R, Graf N, Johansen P, Kundig TM. Intralymphatic allergen administration renders specific immunotherapy faster and safer: a randomized controlled trial. Proc Natl Acad Sci U S A. 2008; 105(46):17908–12. [PubMed: 19001265]
41. Shah P, Desai P, Patel A, Singh M. Skin permeating nanogel for the cutaneous co-delivery of two anti-inflammatory drugs. Biomaterials. 2012; 33(5):1607–1617. [PubMed: 22118820]
42. Lawler SE, Speranza M, Cho C, Chiocca E. Oncolytic viruses in cancer treatment: A review. JAMA Oncology. 2016
43. Cornell RC, Greenway HT, Tucker SB, Edwards L, Ashworth S, Vance JC, Tanner DJ, Taylor EL, Smiles KA, Peets EA. Intralesional interferon therapy for basal cell carcinoma. J Am Acad Dermatol. 1990; 23(4):694–700. [PubMed: 2229497]
44. Edwards L, Whiting D, Rogers D, Luck K, Smiles KA. The effect of intralesional interferon gamma on basal cell carcinomas. J Am Acad Dermatol. 1990; 22(3):496–500. [PubMed: 2107219]
45. Zamarin D, Holmgaard RB, Subudhi SK, Park JS, Mansour M, Palese P, Merghoub T, Wolchok JD, Allison JP. Localized Oncolytic Virotherapy Overcomes Systemic Tumor Resistance to Immune Checkpoint Blockade Immunotherapy. Sci Transl Med. 2014; 6(226):226ra32–226ra32.
46. Kamath AT, Henri S, Battye F, Tough DF, Shortman K. Developmental kinetics and lifespan of dendritic cells in mouse lymphoid organs. Blood. 2002; 100(5):1734–1741. [PubMed: 12176895]
47. Kissenpfennig A, Henri S, Dubois B, Laplace-Builhe C, Perrin P, Romani N, Tripp CH, Douillard P, Leserman L, Kaiserlian D, Saeland S, Davoust J, Malissen B. Dynamics and function of Langerhans cells in vivo: dermal dendritic cells colonize lymph node areas distinct from slower migrating Langerhans cells. Immunity. 2005; 22(5):643–54. [PubMed: 15894281]
48. Thomas SN, Rutkowski JM, Pasquier M, Kuan EL, Alitalo K, Randolph GJ, Swartz MA. Impaired Humoral Immunity and Tolerance in K14-VEGFR-3-Ig Mice That Lack Dermal Lymphatic Drainage. J Immunol. 2012; 189(5):2181–2190. [PubMed: 22844119]
49. Thomas SN, Schudel A. Overcoming transport barriers for interstitial-, lymphatic-, and lymph node-targeted drug delivery. Curr Opin Chem Eng. 2015; 7:65–74. [PubMed: 25745594]
50. Randolph GJ, Angeli V, Swartz MA. Dendritic-cell trafficking to lymph nodes through lymphatic vessels. Nat Rev Immunol. 2005; 5(8):617–628. [PubMed: 16056255]
51. Wu F, Bhansali SG, Law WC, Bergey EJ, Prasad PN, Morris ME. Fluorescence imaging of the lymph node uptake of proteins in mice after subcutaneous injection: molecular weight dependence. Pharm Res. 2012; 29(7):1843–53. [PubMed: 22373666]
52. Reddy ST, Berk DA, Jain RK, Swartz MA. A sensitive in vivo model for quantifying interstitial convective transport of injected macromolecules and nanoparticles. J Appl Physiol. 2006; 101(4): 1162–1169. [PubMed: 16763103]
53. Uto T, Toyama M, Nishi Y, Akagi T, Shima F, Akashi M, Baba M. Uptake of biodegradable poly(γ-glutamic acid) nanoparticles and antigen presentation by dendritic cells in vivo. Results Immunol. 2013; 3:1–9. [PubMed: 24600553]
54. Platt AM, Rutkowski JM, Martel C, Kuan EL, Ivanov S, Swartz MA, Randolph GJ. Normal dendritic cell mobilization to lymph nodes under conditions of severe lymphatic hypoplasia. J Immunol. 2013; 190(9):4608–20. [PubMed: 23530147]

55. Guo D, Li J, Xie G, Wang Y, Luo J. Elastic Properties of Polystyrene Nanospheres Evaluated with Atomic Force Microscopy: Size Effect and Error Analysis. Langmuir. 2014; 30(24):7206–7212. [PubMed: 24892186]

56. Bippes CA, Humphris ADL, Stark M, Müller DJ, Janovjak H. Direct measurement of single-molecule viscoelasticity in atomic force microscope force-extension experiments. Eur Biophys J. 2006; 35(3):287–292. [PubMed: 16237549]

57. Radiom M, Honig CDF, Walz JY, Paul MR, Ducker WA. A correlation force spectrometer for single molecule measurements under tensile load. J Appl Phys. 2013; 113(1):013503.

58. Babu S, Fan C, Stepanskiy L, Uitto J, Papazoglou E. Effect of size at the nanoscale and bilayer rigidity on skin diffusion of liposomes. J Biomed Mater Res, Part A. 2009; 91(1):140–148.

59. Longmire MR, Ogawa M, Choyke PL, Kobayashi H. Biologically optimized nano-sized molecules and particles: more than just size. Bioconjugate Chem. 2011; 22(6):993–1000.

60. Arnida, Janát-Amsbury MM, Ray A, Peterson CM, Ghandehari H. Geometry and Surface Characteristics of Gold Nanoparticles Influence their Biodistribution and Uptake by Macrophages. Eur J Pharm Biopharm. 2011; 77(3):417–423. [PubMed: 21093587]

61. Muro S, Garnacho C, Champion JA, Leferovich J, Gajewski C, Schuchman EH, Mitragotri S, Muzykantov VR. Control of endothelial targeting and intracellular delivery of therapeutic enzymes by modulating the size and shape of ICAM-1-targeted carriers. Mol Ther. 2008; 16(8):1450–8. [PubMed: 18560419]

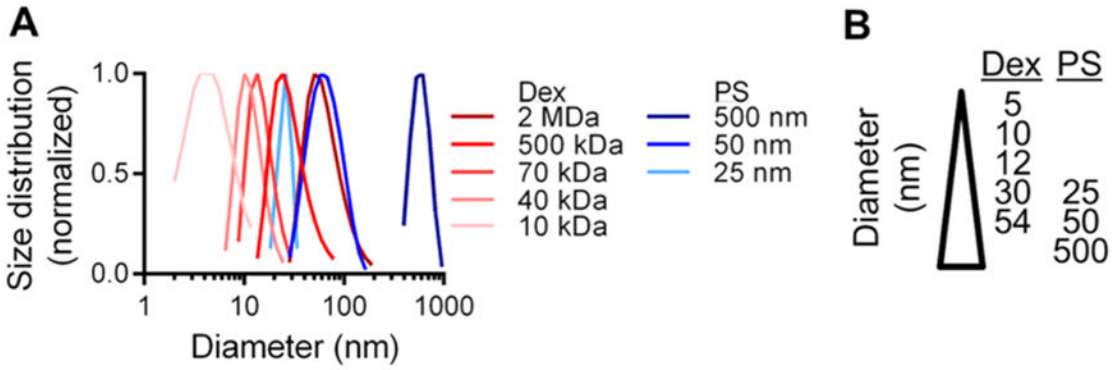

Figure 1.

(A) Measured hydrodynamic sizes of fluorescent dextran (Dex) and polystyrene sphere (PS) and (B) tracer panel.

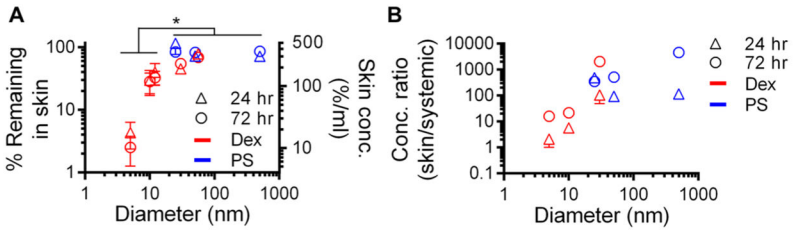

Figure 2.

Tracer retention in skin injection site increases with macromolecular but not particle hydrodynamic size but relative enrichment relative to systemic tissues increases with size for all tracer forms. (A) Percent of injection amount and resulting concentration of tracer within the dermal injection site 24 and 72 h p.i. (B) Ratio of tracer concentrations within the injected skin versus systemic tissues (spleen, lungs, liver, and kidneys) 24 and 72 h p.i. * indicates significance for 5–12 vs 25, 50, 54, and 500 nm tracers at 24 and 72 h p.i. by one-way ANOVA and posthoc Fisher's LSD tests.

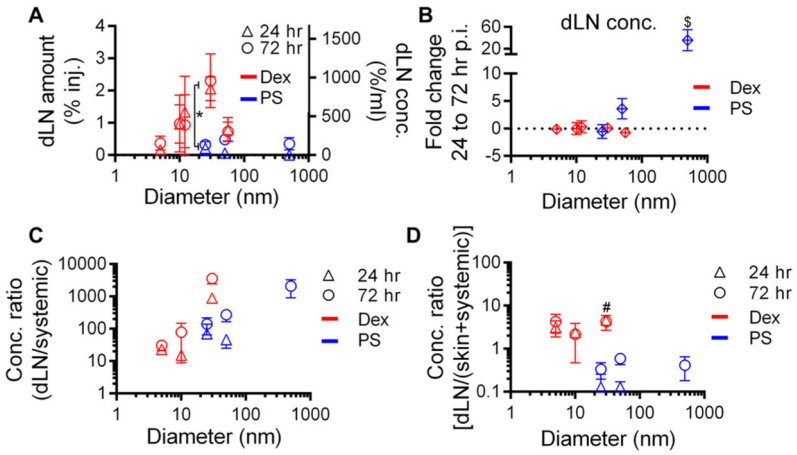

Figure 3.

Tracer accumulation within dLN is greatest for macromolecules, increases most appreciably over time with increasing particle size, and is the most specifically enriched relative to other tissues for macromolecules. (A) Percent of injection amount and resulting concentration of tracer within dLN after dermal injection 24 and 72 h p.i. (B) Fold change in dLN tracer concentrations from 24 to 72 h p.i. (C) Ratio of accumulated tracer concentrations within the dLN versus systemic tissues at 24 and 72 h p.i. (D) Tracer accumulation within dLN versus the skin injection site and systemic tissues at 24 and 72 h p.i. * indicates significant for 25 vs 30 nm tracers by Mann–Whitney *U* tests, $ indicates significance for 500 vs 50 and 25 nm tracers, and # indicates significance for 30 vs 25, 50, and 500 nm tracers at 24 and 72 h by one-way ANOVA and posthoc Fisher's LSD tests. The level of 500 nm tracer accumulation within dLN at 24 h p.i. was not detectable.

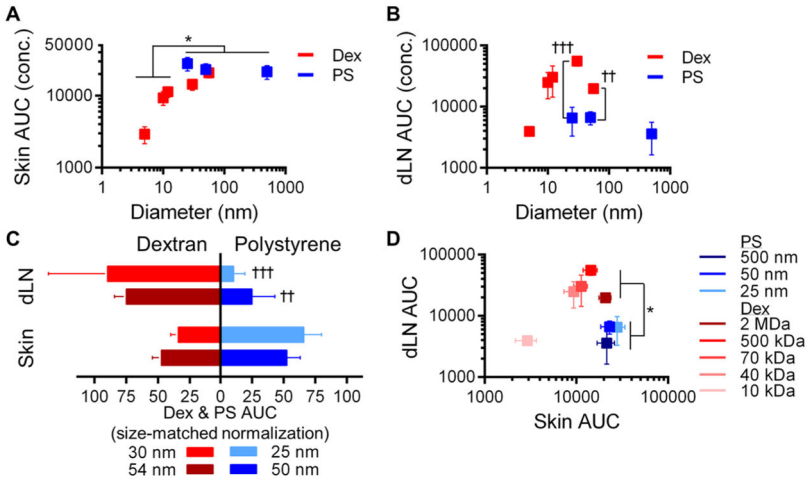

Figure 4.

Tracer exposure within dLN and skin is size and form dependent. AUC of measured concentration profiles from 0 to 72 h p.i. in (A) skin and (B) dLN. (C) Tissue exposure for size-matched dextran (red) and polystyrene spheres (blue) as percentage of total for both forms for the skin (left) and dLN (right). (D) AUC of tracers in skin and dLN. * indicates significant for 5–12 vs 25, 50, and 500 nm tracers by by one-way ANOVA and posthoc Fisher's LSD tests, † indicates significance for 30 vs 25 and 54 vs 50 nm tracers by Mann–Whitney *U* tests.